Journal of
Applied and Computational Mechanics

Shahid Chamran
University of Ahvaz

Research Paper

VIV Control Strategies Using Displacement-Based Phenomenological Model

Muhammad R. Hajj[1], Arshad Mehmood[2], Imran Akhtar[3], Khondokar Billah[1]

[1] Department of Civil, Environmental and Ocean Engineering, Stevens Institute of Technology, Hoboken, NJ, USA, Email(s): mhajj@stevens.edu, kbillah@stevens.edu

[2] Department of Mechanical Engineering, University of Engineering and Technology, Peshawar, Pakistan, Email: marshad@vt.edu

[3] Department of Mechanical Engineering, National University of Sciences and Technology, Islamabad, Pakistan, Email: imranvt@gmail.com

Abstract. Linear and nonlinear feedback control of vortex-induced vibrations are assessed using a single degree-of-freedom phenomenological model of the uncontrolled response. The model is based on the role of linear and nonlinear damping forces in inducing and limiting the amplitude of these vibrations. First, the model prediction is validated using data from previously published high-fidelity direct numerical simulations. Then, linear and nonlinear control are applied to the validated model over a broad range of gain values. The predicted controlled responses are also validated against previously published results from high-fidelity numerical simulations. Based on this validation, it is shown that the single degree-of-freedom model is an effective alternative, in terms of computational cost, to high fidelity simulations in assessing control strategies over broad regions of control gains.

Keywords: Vortex-induced vibrations, Reduced-order model, Linear and nonlinear control.

1. Introduction

The periodic shedding of positive and negative vorticity from a cylinder when placed in a uniform flow subjects it to oscillatory lift and drag forces. If the cylinder is allowed to move under the action of these forces, the motion influences the flow, which impacts the magnitude and direction of the oscillatory forces. Based on the structure's stiffness, damping, and mass and for specific fluid density and viscosity, the extent of the coupling between the flow and the cylinder's motion depends on the flow velocity, which determines the frequency of the vortex shedding. Of particular interest is the flow regime where the motion of the cylinder synchronizes the vortex shedding frequency, which results in large-amplitude oscillations or vortex-induced-vibrations (VIV). This regime is referred to as lock-in or synchronization regime. The synchronization phenomenon has been documented in many experimental and numerical studies. Sarpkaya [1] discussed parameters that influence VIV, the unsteady forces acting on the cylinder, and the linearized equations of the self-excited motion and their limitations, especially when the oscillations exhibit amplitude and phase modulations. Gabbai and Benaroya [2] discussed an approach based on variational principles to derive a governing equation for VIV [3] and reviewed other semi-empirical models that predict the response of the cylinder to the forces from the flow. Williamson and Govardhan [4] reviewed important aspects impacting the VIV including the vortex dynamics and energy transfer that cause the vibrations, and the significance of mass ratio, damping and effective elasticity.

Because large-amplitude oscillations cause structural fatigue and can ultimately lead to failure, there has been significant interest in characterizing the VIV as a phenomenon and in reducing its impact through different control strategies. Passive control can be achieved by varying the flow through geometrical changes or the addition of appendages to the surface of the cylinder, e.g. streamline fairing, tripping wire, or helical strake to reduce the impact of the vortex shedding pattern [5], or by increasing the structural damping [6] or the addition of a secondary device, e.g. an energy sink [7, 8] to absorb the energy that is transferred from the flow to the cylinder. In contrast to passive control approaches, active control suppresses the vibrations by balancing the cylinder's motion with external energy that is supplied to the flow, e.g. blowing and suction [9,10] or acoustic feedback [11-13], or to the cylinder, e.g. feedback control [14,15].

Evaluation of different control strategies is usually performed or assessed through experiments or numerical simulations. Yet, when performing optimization under different constraints over a large design space, the experiments may not be effective, and the computational cost of high-fidelity simulations may be prohibitive. In contrast, simplified or reduced-order models can be used for effective evaluation of control strategies. Different VIV-reduced order models have been suggested. The simplest of these models is the single degree-of-freedom model with sinusoidal representation of the fluid forces on the right-hand side of the cylinder's governing equation of motion. In other models, the cylinder's equation of motion is coupled with a wake oscillator model that predicts the fluid force on the cylinder. A third set of models relies on determining the force components from measurements or simulations. Each of the above representations has its shortcomings. For instance, algebraic representation of the fluid forces is not

accurate because it does not account for memory effects associated with the vortex shedding and wake. Although representing the force by a nonlinear oscillator is advantageous over the algebraic representation because it accounts for nonlinearities associated with flow separation and wake effects, determining its form and parameters and representing its coupling with the cylinder's equation of motion are challenging.

Towards overcoming these challenges, we use a single degree-of-freedom model that directly represents vortex-induced vibrations of a freely oscillating cylinder with the displacement as the only variable [16]. The basis of the proposed model is that positive excitation in the form of negative fluid damping, represented by a force proportional to the cylinder's velocity, is required to induce the self-excited oscillations [17] and that nonlinear damping is required to limit the amplitude of these oscillations. We demonstrate the effectiveness of the proposed model in implementing linear and nonlinear feedback control by comparing its predictions with previously reported data from high-fidelity simulations [15]. The rest of the paper is structured as follows: the phenomenological model and approach to identify its parameters are presented in section 2. Details of the direct numerical simulation used to generate the time series for identification of the parameters of the phenomenological model are presented in in section 3. The control results including required gains and power for implementing linear and nonlinear velocity feedback control are validated and discussed in section 4. The conclusions are drawn in section 5.

2. Phenomenological Model

2.1 Governing equation

The governing equation of an elastically mounted rigid cylinder having a mass m_{cyl}, structural damping c, and stiffness k that is allowed to freely vibrate in the transverse direction when placed in a uniform flow is written as:

$$m_{cyl}\ddot{y} + c\dot{y} + ky = F_y(t) \tag{1}$$

where y is the transverse displacement of the cylinder, the overdot is used to represent time derivative, and $F_y(t)$ is the flow-induced transverse force acting on the cylinder as shown in fig. 1. In the case of a stationary cylinder, this force coincides with the lift force and is determined by the vortex shedding. It has one dominant frequency component, which is the frequency of the vortex shedding. In the lock-in region, the natural frequency of the cylinder matches that of the vortex shedding, which results in finite-amplitude oscillations or VIV. Because the relative velocity of the cylinder to that of the incident flow is time-varying, the lift and drag forces continuously change directions depending on the instantaneous angle of attack, $\theta(t)$, between the x-axis and the direction of the instantaneous velocity vector, V. Consequently, both lift and drag forces contribute to the transverse force such that $F_y(t) = F_D(t)\sin\theta + F_L(t)\cos\theta$ as shown in the schematic presented in Fig. 1.

At the onset of the vibrations, the angle θ is small because the transverse velocity of the cylinder is much smaller than the incident velocity. As such, we write:

$$\sin\theta \cong \tan\theta = \frac{\dot{y}}{U_\infty} \tag{2}$$

Subsequently, the instantaneous drag force is proportional to the transverse velocity of the cylinder. The instantaneous lift is out of phase with the drag and is proportional to the acceleration of the cylinder. This latter component is represented by the added mass, m_{add}. As for the component that is proportional to the velocity, it must be positive to initiate energy transfer from the flow to the cylinder and result in the self-excited oscillations. Because of its dependence on the velocity, this positive excitation is effectively a negative linear damping force. In addition to this linear force, flow nonlinearities, which have their source in the flow separation and wake, result in limiting the amplitude of the oscillations. As such, we represent the flow-induced hydrodynamic force by two components that are respectively proportional to the velocity of the cylinder and to its cube value. Using this representation, it is postulated that the vortex-induced vibration of an elastically mounted cylinder when placed in a uniform flow can be represented by a phenomenological model having the form of the Rayleigh oscillator and written as [16]:

$$m\ddot{y} + c\dot{y} + ky = a\dot{y} + b\dot{y}^3 \tag{3}$$

where $m = m_{cyl} + m_{add}$. The coefficients a and b are used to represent the dependence of the transverse force on the velocity and its cubic value, respectively.
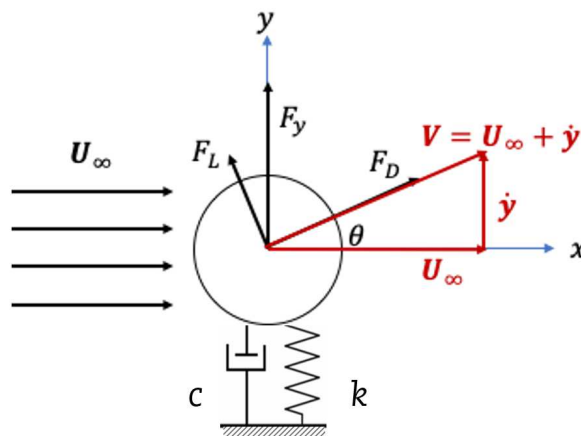

Fig. 1. Schematic of transverse vortex-induced vibrations of a circular cylinder.

Using the incident speed, U_∞, and the cylinder diameter, D, we nondimensionalize eq. (4), which yields

$$\ddot{Y} - 2(\zeta_f - \zeta_d)\frac{2\pi}{U_r}\dot{Y} + \left(\frac{2\pi}{U_r}\right)^2 Y + (\beta_f)\frac{U_r}{2\pi}\dot{Y}^3 = 0 \tag{4}$$

where $Y = y/D$ and the time derivative is performed using the nondimensional time $t^* = tU_\infty/D$. The reduced velocity is defined as $U_r = U_\infty/fD$ where f is the frequency of the cylinder's oscillations, which is set by its natural frequency in the lock-in region. Using the cylinder's natural frequency given by $\omega = \sqrt{k/m}$, the damping ratios associated with the negative damping ratios proportional to the velocity of the cylinder and structural damping are respectively defined as $\zeta_f = a/2m\omega$ and $\zeta_d = c/2m\omega$. The parameter $\beta_f = bD^2\omega/2m$ defines the nondimensional nonlinear damping force by the flow. It is important to note that this model is valid only in cases where VIV results from lock-in. It may not be applicable in VIV that does not involve or require lock-in as in the case of low values of the mass ratio defined as the ratio of the cylinder density to fluid density.

2.2 Identification of Model Parameters

Identification of the fluid damping coefficients is performed using data from direct numerical simulation of vortex-induced vibrations. The identification procedure, as detailed in [16], involves combining an approximate solution of eq. (4) with spectral analysis of data from the numerical simulations. Using the method of multiple scales [18-20], the approximate solution of eq. (4) is written as:

$$Y = A_1 \cos\left(\frac{2\pi}{U_r}t^* + \varphi\right) + \frac{\beta_f}{32}A_1^3 \cos\left(3\frac{2\pi}{U_r}t^* + 3\varphi - \frac{\pi}{2}\right) \tag{5}$$

where φ is a constant phase and A_1, which represents the amplitude of the first harmonic response, is determined from the modulation equation

$$\dot{A}_1 = (\zeta_f - \zeta_d)A_1 - \frac{3}{8}\beta_f A_1^3 \tag{6}$$

Under steady-state conditions $\dot{A}_1 = 0$. The ratio of the linear and nonlinear damping is then given by

$$\frac{\zeta_f - \zeta_d}{\beta_f} = \frac{3}{8}A_1^2 \tag{7}$$

The amplitude of the third harmonic of the response A_3, as noted from eq. (5), is given by

$$A_3 = \frac{\beta_f}{32}A_1^3 \tag{8}$$

In the identification procedure, we will use A_1 and A_3 as determined from the spectral analysis of the time series as obtained from a high-fidelity simulation to determine the nonlinear fluid damping coefficient β_f. Then, we use eq. (7) to identify the linear fluid damping coefficient ζ_f.

3. Numerical Simulation of Uncontrolled Vortex-Induced-Vibrations

3.1 Governing Equations and Simulation Approach

Details of the numerical simulation used to generate time series for the identification of the model parameters, as proposed above, are provided in [10, 21-24]. The accelerating reference frame (ARF) computational approach whereby the computational mesh of the flow field is fixed to the cylinder and allowed to move in space is used to solve the governing equations. This requires adjusting the momentum equations and boundary conditions as appropriate. As such, the cylinder's motion in response to the force exerted on it by the flow is governed in an inertial reference frame by the nondimensional equation:

$$\ddot{Y} + 2\zeta_d\frac{2\pi}{U_r}\dot{Y} + \left(\frac{2\pi}{U_r}\right)^2 Y = \frac{2}{\pi m^*}C_Y \tag{9}$$

where m^* is the ratio of the cylinder's mass to that of the fluid it replaced, and C_Y is the force coefficient in the transverse direction. The nondimensionalized equations governing this field in the reference frame attached to the cylinder are given by:

$$\frac{\partial u_i}{\partial x_i} = 0 \tag{10}$$

and

$$\frac{\partial u_i}{\partial t} + \frac{\partial}{\partial x_j}(u_j u_i) = \frac{\partial p}{\partial x_i} + \frac{1}{Re}\frac{\partial^2 u_i}{\partial x_j \partial x_j} - \ddot{Y}_i \tag{11}$$

where $i, j = 1, 2, 3$, u_i represents the Cartesian velocity components, p is the pressure and $Re = U_\infty D/\nu$ is the Reynolds number. We note that the equations governing the fluid flow are coupled with those governing the cylinder's motion through the cylinder's (or frame) acceleration $\ddot{Y}_i$. Implementing the ARF requires adjusting the domain boundary conditions to include the effects of the moving cylinder. The force coefficient, C_Y, is obtained by integrating the surface and viscous stresses over the surface of the cylinder. A second-order central-difference scheme is used for all spatial derivatives except for convective terms. Time advancement

is performed using a fractional step approach where a predictor step calculates an intermediate velocity field, and a corrector step updates the velocity by satisfying the pressure-Poisson equation at the new time step. The diagonal viscous terms are advanced implicitly using the second-order accurate Crank-Nicolson method, whereas all of the other terms are advanced using the second-order accurate Adams-Bashforth method. A predictor-corrector scheme is used to solve the coupled problem defined by eq. (9), (10) and (11). In this scheme, the fluid force, from eq. (11) is used in the governing equation of the motion of the cylinder. The predicted position of the cylinder is then used in the flow simulation to compute an updated fluid load. This load is then used to compute a new position for the cylinder, using the corrector scheme. These steps are repeated until a match, based on a specified conditional error at each time step, between the fluid force and the cylinder motion is achieved. As reported by [10, 21-24], the fluid flow solver and coupling scheme were validated with previous experimental and numerical results.

3.2 Identification of Fluid Damping Coefficients

To identify the coefficients of the reduced-order model, the numerical simulation in the lock-in region was performed over a computational domain of $25D$ using an "O" type grid with a resolution of 192x252 grid points in the radial and tangential directions, respectively. Time integration was carried out with a time step $\Delta t = 0.002$. The simulation was performed for a cylinder having a mass ratio $m^* = 149.1$ and a damping ratio $\zeta_d = 0.0012$ at $Re = 106$, which falls in the lock-in regime [10,21-24]. Simulated time series and spectra of the transverse force coefficient, C_Y, and cylinder displacement, Y are presented in fig. 2. The force coefficient has an amplitude of 1.31 and its spectrum shows peaks at a fundamental frequency and its odd harmonics. The first peak is at the oscillation (or vortex shedding) nondimensional frequency $f = 1/U_r = 0.168$, where U_r is the reduced velocity. It has a spectral amplitude of 1.27. The second is at the third harmonic of 0.505 with a spectral amplitude of 0.032. The third peak at the fifth harmonic has a much smaller magnitude. The time series of the nondimensional displacement shows an amplitude of 0.418. Its respective spectrum shows a peak also at 0.168 that has an amplitude $A_1 = 0.418$. Although no clear peak is present at the third harmonic in the displacement spectrum, the spectral amplitude at the third harmonic is $A_3 = 0.00037$.

Given the values from the spectral analysis, we estimate the nonlinear damping coefficient as

$$\beta_f = \frac{32A_3}{A_1^3} = 0.1574 \tag{12}$$

and the linear damping coefficient as

$$\zeta_f = \frac{3}{8}\beta_f A_1^2 + \zeta_d = 12\frac{A_3}{A_1} + \zeta_d = 0.0115 \tag{13}$$

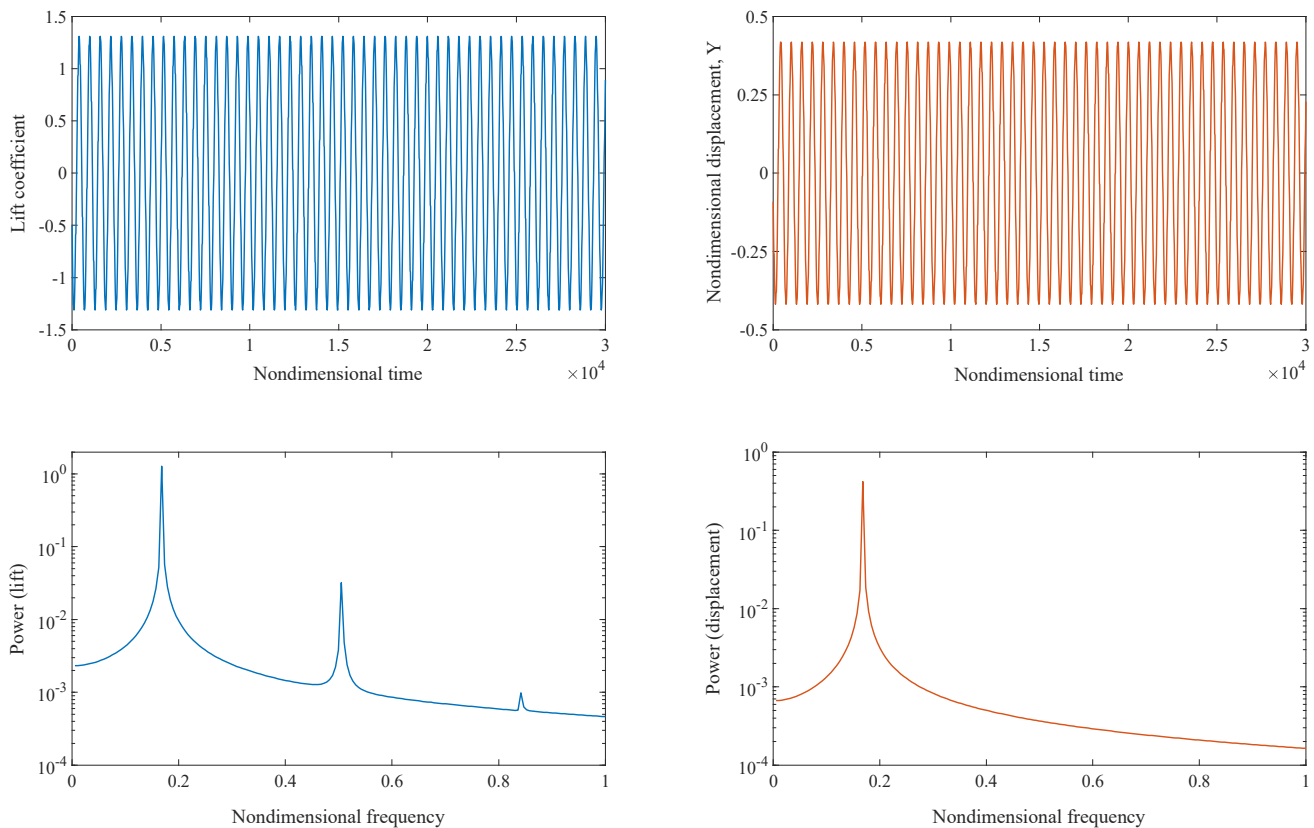or, for $\zeta_d = 0.0012$, the fluid damping $\zeta_f = 9.58\zeta_d$.

Fig. 2. Top: Direct numerical simulation of the lift coefficient and uncontrolled nondimensional transverse displacement of the cylinder undergoing vortex-induced vibrations. Bottom: respective spectral density functions of the time series.
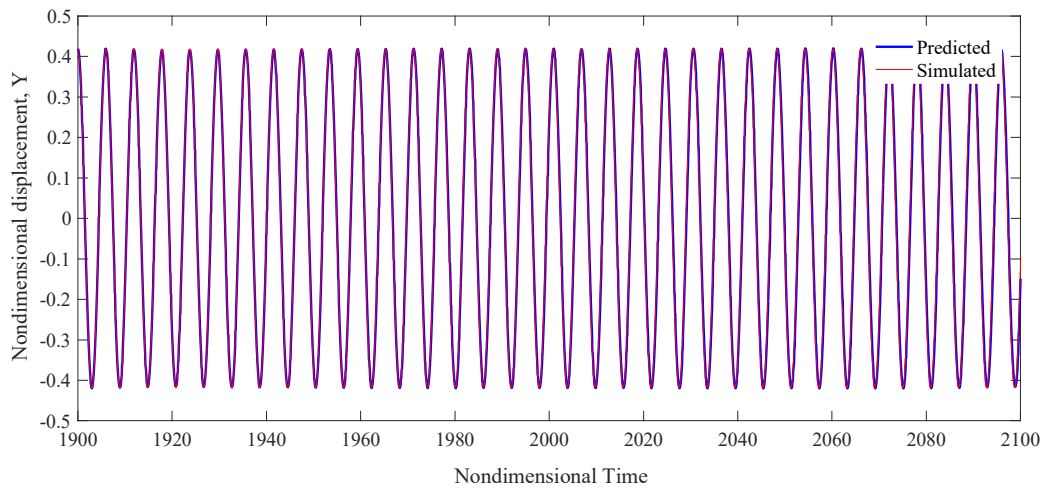
Fig. 3. Validation of predicted nondimensional displacement using the reduced-order model through comparison with displacement from high-fidelity numerical simulations.

Validation of the model is demonstrated by comparing the time series of the nondimensional displacement as obtained from the numerical simulation with those obtained by numerically integrating eq. (4) using the identified coefficients. Figure 3 shows perfect agreement, in terms of steady-state amplitude and frequency of the time series predicted from the model with the time series obtained from the high-fidelity numerical simulation.

4. Control of Vortex Induced Vibrations

4.1 Implementation using the Phenomenological Model

Introducing linear and nonlinear cubic velocity feedback control into the governing equation yields

$$\ddot{Y} - 2\left(\frac{\zeta_f - \zeta_d}{1 + \zeta_{kl}/\zeta_d}\right)\frac{2\pi}{U_r}\dot{Y} + \left(\frac{2\pi}{U_r}\right)^2 Y + \beta_f\left(1 + \frac{\beta_{kc}}{\beta_f}\right)\frac{U_r}{2\pi}\dot{Y}^3 = 0 \tag{14}$$

where ζ_{kl} and β_{kc} are used to represent the nondimensional respective gains of the linear and cubic velocity feedback controllers. The linear velocity feedback control should reduce the impact of the negative flow damping force that initiates the energy transfer from the flow to the cylinder. As for the nonlinear velocity feedback control, we note that limiting the oscillations in VIV is due to nonlinear damping flow forces generated by the flow separation, vortex shedding and the cylinder's wake. As such, the nonlinear velocity feedback control should be very effective in controlling or reducing the oscillations amplitude. Figure 4 shows time series of the nondimensional displacement for different gain values of the linear controller. Percentage reductions of 38%, 52%, and 98% from the uncontrolled response amplitude of 0.418 are respectively realized for gain values of 0.05 kg/s (or $\zeta_{kl} = 1.58\zeta_d$), 0.1 kg/s (or $\zeta_{kl} = 3.15\zeta_d$), and 1 kg/s (or $\zeta_{kl} = 31.5\zeta_d$). Clearly, reducing the oscillations amplitude from about 40% to total suppression requires increasing the gain of linear controller by two orders of magnitude. Figure 5 shows time series of the nondimensional displacement for different gain values of the nonlinear controller. Percentage reductions of 28%, 47%, and 99% from the uncontrolled response amplitude of 0.418 are respectively realized for gain values of 100 Ns³/m³ (or $\beta_{kc} = 0.12$), 1000 Ns³/m³ (or $\beta_{kc} = 1.18$), and 1x 10⁶ Ns³/m³ (or $\beta_{kc} = 1183$). In contrast to the case of linear controller, reducing the oscillation amplitudes from about 50% to total suppression requires an increase in the gain of the nonlinear control by three orders of magnitude. This difference will be further considered by comparing the power required for different levels of magnitude reductions using both control strategies.
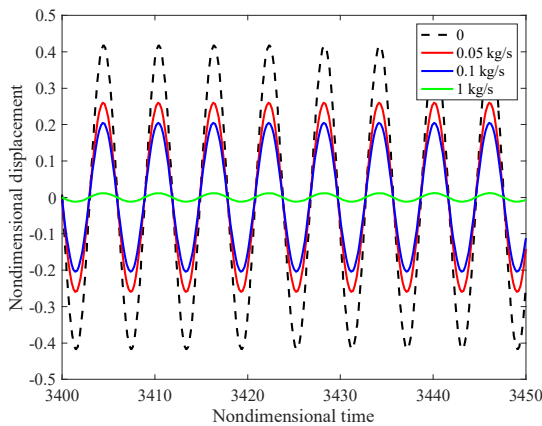

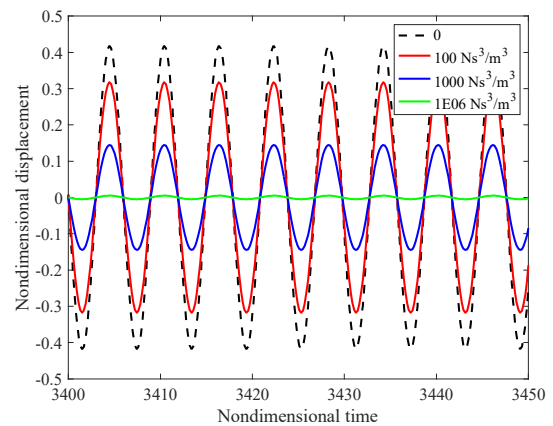**Fig. 4.** Time series of nondimensional cylinder displacement for increased gain values of linear controller.

Fig. 5. Time series of nondimensional cylinder displacement for increased gain values of nonlinear controller.
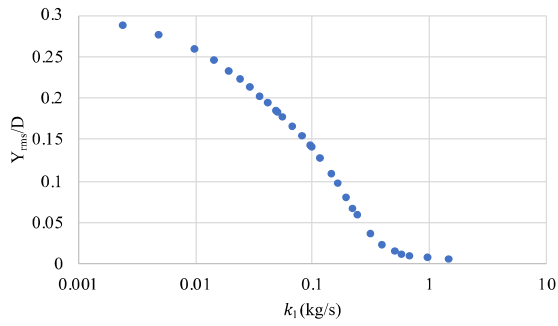
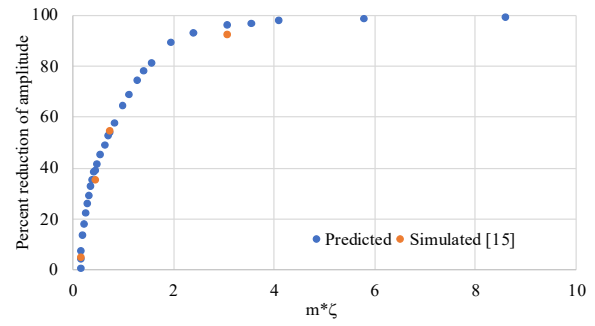**Fig. 6.** Reduction in RMS amplitude of oscillations as linear gain is increased.

Fig. 7. Validation of percent reduction for different values of linear gain with high fidelity simulations [15].
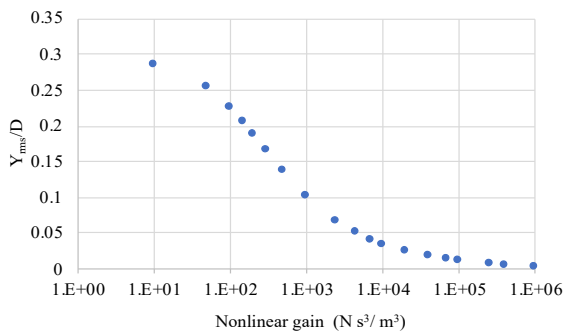

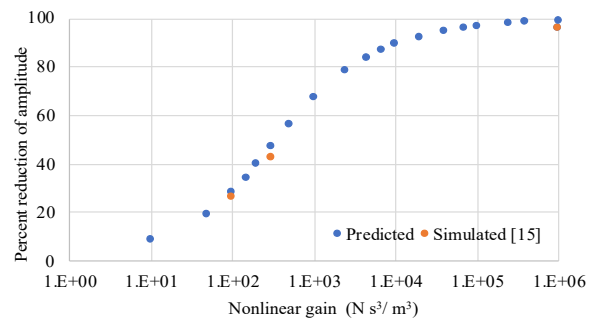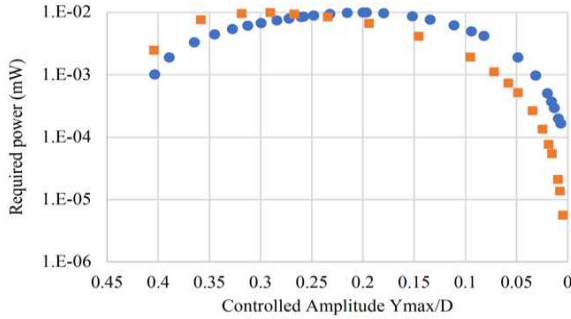**Fig. 8.** Reduction in RMS amplitude of oscillations as nonlinear gain is increased.

Fig. 9. Validation of percent reduction for different values of nonlinear gain with high fidelity simulations [15].

Fig. 10. Variation of the required nondimensional power (in mW) as a function of the nondimensional controlled displacement. Circles and squares correspond to required power by linear and nonlinear controllers, respectively. Data shows agreement with simulated results (figure 10 of [15]).
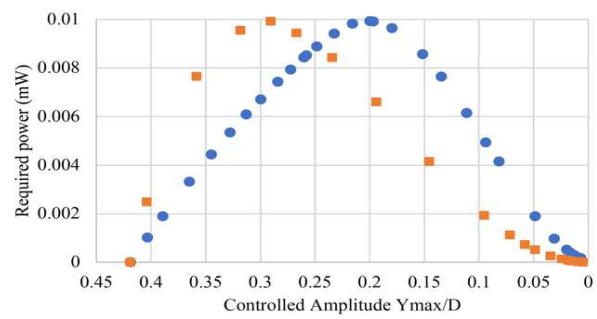

Fig. 11. Variation of the required nondimensional power (in mW) as a function of the nondimensional controlled displacement. Circles and squares correspond to required power by linear and nonlinear controllers, respectively.

More details about the gain required to achieve specific levels of amplitude reduction can be obtained from the variations of the normalized *rms* amplitude of the cylinder oscillations over a broader range of gain values. The plot in fig. 6 shows that the rate at which the oscillations amplitude is reduced increases as the gain of the linear controller is increased up to the point where the normalized amplitude is 0.05. Below this value, amplitude reduction towards total suppression will require significant increase in the linear gain. The validity of the results is noted on the basis of the data presented in fig. 7, which shows the percent reduction of the oscillation amplitudes as a function of the combined mass-damping parameter. Predicted reductions from high fidelity simulations [15] at four values of the mass-damping parameter are within 3% of predicted values using the phenomenological model.

Figures 8 and 9 show the drop in the nondimensional response for different gain values β_{kc} of the nonlinear controller. The data in both plots show that the highest rate of reduction takes place in an intermediate range of gain values and that total suppression will require an increase of this value by three order of magnitudes beyond this range. The data in fig. 9 show agreement between predicted reductions from the phenomenological model and those obtained from high-fidelity simulations as reported in [15].

One measure of the efficiency of both controllers is the required power, which is given by [15]:

$$P_{Lavg} = \frac{1}{2} K_l A_{L1}^2 D^2 \omega_n{}^2 \tag{15}$$

for the linear controller, and

$$P_{NLavg} = \frac{3}{8} K_c A_{NL1}^4 D^4 \omega_n{}^4 \tag{16}$$

for the nonlinear controller. Figures 10 and 11 show a comparison of these values. The plot in figure 10 is quantitatively in agreement with the results reported from the high-fidelity simulations [15]. More details can be noted from figure 10, which shows that linear control is more effective in reducing the high amplitude oscillations ($Y_{max}/D > 0.25$) while nonlinear control is more effective in reducing the lower amplitude oscillations ($Y_{max}/D < 0.25$). For instance, reducing the amplitude by 20 % using nonlinear control requires almost 50% more power than using linear control. On the other hand, reducing it by 80% using nonlinear control requires only half the power that is required by the linear controller. The reason is that limiting the lower amplitude oscillations requires significantly less power than limiting the higher amplitude oscillations.

5. Conclusions

We demonstrated the effectiveness of using a recently proposed single degree-of-freedom model that directly predicts the displacement in vortex-induced vibrations in assessing capabilities of linear and nonlinear control strategies. Both model and controlled amplitude levels for specific gains were validated using previously published data from higher fidelity simulations. The results show that the linear control requires less external power to reduce the amplitude of the oscillations by up to 50%. Reducing the amplitude to lower levels can be achieved more effectively using a nonlinear controller. Still, the required gain for the nonlinear controller is very large and may not be practical. Of particular interest is that the validated control results were obtained in few hours, which constitute a small fraction of the weeks required to perform the equivalent high fidelity numerical simulations.

Author Contributions

M. Hajj planned the analysis and initiated the project; A. Mehmood and I. Akhtar performed and validated the numerical simulations; K. Billah supported the analysis and validation. The manuscript was written through the contribution of all authors. All authors discussed the results, reviewed and approved the final version of the manuscript.

Conflict of Interest

The authors declared no potential conflicts of interest with respect to the research, authorship and publication of this article.

Funding

References

[1] Sarpkaya, T., Vortex induced oscillations: a selective review, *Journal of Applied Mechanics*, 46(2), 1979, 241–258.
[2] Gabbai, R., Benaroya, H., An overview of modeling and experiments of vortex-induced vibration of circular cylinders, *Journal of Sound and Vibration,* 282, 2005, 575-616.
[3] Dong, P., Benaroya, H., Wei, T., Integrating experiments into an energy-based reduced-order model for vortex induced-vibrations of a cylinder mounted as an inverted pendulum, *Journal of Sound and Vibration*, 276(1–2), 2004, 45–63.
[4] Williamson C., Govardhan R., Vortex-Induced Vibrations, *Annual Review of Fluid Mechanics*, 36, 2004, 413–455.
[5] Zdravkovich M.M., Review and classification of various aerodynamic and hydrodynamic means for suppressing vortex shedding, *Journal of Wind Engineering and Industrial Aerodynamics*, 7, 1981, 145–189.
[6] Walshe D.E., Wootton L.R., Preventing wind-induced oscillations of structures of circular section, *Proceedings of the Institution of Civil Engineers*, 47, 1979, 1–24.
[7] Tumkur, R.K.R., Domany, E., Gendelman, O.V., Masud, A., Bergman, L.A., Vakakis, A.F., Reduced-order model for laminar vortex-induced vibration of a rigid circular cylinder with an internal nonlinear absorber, *J. Commun. Nonlinear Sci. Numer. Simul.*, 18, 2013, 1916–1930.
[8] Mehmood A., Nayfeh A.H., Hajj M.R., Effects of a non-linear energy sink (NES) on vortex-induced vibrations of a circular cylinder, *Nonlinear Dynamics*, 77, 2014, 667–680.
[9] Akhtar I., Nayfeh A.H., On controlling the bluff body wake using a reduced-order model, *Proceedings of the 4th Flow Control Conference*, AIAA-2008-4189, Seattle, WA, 2018.
[10] Akhtar I., *Parallel Simulations, Reduced-order Modeling, and Feedback Control of Vortex Shedding using Fluidic Actuators,* Ph.D. Thesis, Department of Aerospace Engineering, Virginia Polytechnic Institute and State University, Blacksburg, VA, 2008.
[11] Blevins R.D., The effect of sound on vortex shedding from cylinders, *Journal of Fluid Mechanics*, 161, 1985, 217–237.
[12] Fowcs Williams J.E., Zhao B.C., The active control of vortex shedding, *Journal of Fluids and Structures*, 3, 1988 115–122.
[13] Huang X.Y., Feedback control of vortex shedding from a circular cylinder, *Experiments in Fluids*, 20, 1996 218–224.
[14] Baz A., Ro J., Active control of flow-induced vibrations of a flexible cylinder using direct velocity feedback, *Journal of Sound and Vibration*, 146, 1991, 33–45.
[15] Mehmood, A., Abdelkefi, A., Akhtar, I., Nayfeh, A.H., Nuhait, A., Hajj, M.R., Linear and nonlinear active feedback controls for vortex-induced vibrations of circular cylinders, *Journal of Vibration and Control*, 331, 2012, 5774–5787.
[16] Hajj, M.R., Mehmood, A., Akhtar, I., Single degree-of-freedom model of displacement in vortex-induced-vibrations, *Nonlinear Dynamics*, 103, 2021, 1305-1320.
[17] Konstantinidis, E., Zhao, J., Leontini, J., Jacono, D.L., Sheridan, J., Excitation and Damping Fluid Forces on a Cylinder Undergoing Vortex-Induced Vibration, *Frontiers in Physics*, 7, 2019, Article ID 185.

[18] Nayfeh, A.H., *Perturbation Methods*, Wiley, New York, 1973.

[19] Nayfeh, A.H., *Introduction to Perturbation Techniques*, Wiley, New York, 1981.

[20] Nayfeh, A.H., Owis, F., Hajj, M.R., A model for the coupled lift and drag on a circular cylinder. *In ASME 2003 International Design Engineering Technical Conferences and Computers and Information in Engineering Conference*, American Society of Mechanical Engineers Digital Collection, 2003, 1289-1296.

[21] Mehmood, A., Abdelkefi, A., Hajj, M.R., Akhtar, I., Nayfeh, A.H., Nuhait, A., Piezoelectric Energy Harvesting from Vortex-Induced Vibrations of Circular Cylinder, *Journal of Sound and Vibration*, 332(19), 2013, 4656–4667.

[22] Akhtar, I., Elyyan, M., Higher-Order Spectral Analysis to Identify Quadratic Nonlinearities in Fluid-Structure Interaction, *Mathematical Problems in Engineering*, 2018, Article ID 2394124.

[23] Mehmood, A., Abdelkefi, A., Hajj, M.R., Akhtar, I., On the Onset of Bifurcation and Nonlinear Characterization of Vortex-induced Vibrations under Varying Initial Conditions, *Nonlinear Dynamics*, 99(1), 2019, 575-592.

[24] Ghommem, M., Akhtar, I., Hajj, M.R., A low-dimensional tool for predicting force decomposition coefficients for varying inflow conditions, *Progress in Computational Fluid Dynamics*, 13, 2013, 368-381.

ORCID iD

Muhammad R. Hajj https://orcid.org/ 0000-0002-2846-198X

Arshad Mehmood https://orcid.org/ 0000-0003-1723-4500

Imran Akhtar https://orcid.org/ 0000-0001-7522-252X

Khondokar Billah https://orcid.org/ 0000-0001-6626-9959

Publisher's Note Shahid Chamran University of Ahvaz remains neutral with regard to jurisdictional claims in published maps and institutional affiliations.